Protein Import Through the Nuclear Pore Complex Is a Multistep Process

Christopher W. Akey*‡ and David S. Goldfarb*

*Department of Cell Biology, Stanford University School of Medicine, Stanford, California 94305; and
‡Structural Studies Division, Medical Research Council Laboratory of Molecular Biology, Cambridge CB2 2QH, England

Abstract. The transport of macromolecules across the nuclear envelope is mediated by the nuclear pore complex (NPC). Using cryo-electron microscopy and image processing we have mapped the interaction of three specific gold probes with the NPC and obtained projection maps of two possible intermediates in nuclear import. The probes used in these experiments were (*a*) mAb-414, which cross-reacts with *Xenopus* nucleoporins containing O-linked *N*-acetyl glucosamines; (*b*) wheat germ agglutinin, a transport inhibitor; and (*c*) nucleoplasmin, a transport substrate. Strong binding sites of the three probes are circularly arrayed on NPCs between radii of 100 and 125 Å and may be coextensive. These results suggest that nucleoplasmin–gold (NP-gold) can form at least three distinct complexes with a central transport assembly of the NPC, which may represent intermediates of a multistep protein import pathway. Initially, NP-gold appears to bind at multiple sites located around the periphery of the closed NPC transporter and also directly over the center where it can dock. In a subsequent step NP-gold is translocated through the nuclear pore.

THE nuclear envelope is comprised of two concentric membranes overlaying a network of intermediate filaments called the nuclear lamina and is penetrated by the nuclear pore complex (NPC)[1] at regions where the membranes are fused (reviewed in references 22, 37). The NPC is ~1,450–1,500 Å in diameter (2) and displays ~822 symmetry (2, 32, 48). The pore complex is composed of two rings located at the level of the inner and outer nuclear membranes which frame a central spoke assembly (2, 32, 48); connected to the spokes at the center of the NPC is an assembly we describe as the transporter. This study focuses on the role played by the transporter in the binding and translocation of karyophilic (nucleus-seeking) proteins through the nuclear envelope.

A remarkable aspect of NPC-mediated transport, besides its bidirectionality, is the variety and size range of the molecules transported. The pore complex presumably contains sites for both passive and active nucleocytoplasmic transport (8, 39) and possesses a limiting pore size of ~90 Å for passive exchange (38). Furthermore, the NPC appears to actively transport karyophilic gold particles with diameters of at least 260 Å (14, 18) and large unrolled RNP particles (21, 45). What sort of mechanism is capable of governing this process? A number of studies indicate that both the binding of a protein to the NPC and its transfer across the nuclear envelope are dependent on a nuclear localization signal (18, 35, 40). Although there is no consensus sequence for the nuclear localization signal, the SV-40 large T antigen (29–31) and yeast histone 2B targeting signals (34) both contain essential lysine residues which, when mutated to nonbasic amino acids, greatly reduce the efficiency of the signal in transport (31, 43). Moreover, recent work indicates that residues adjacent to the putative nuclear localization sequences of nucleoplasmin (NP) (9, 10) and SV-40 large T antigen (41) may play an important role in transport. The accumulation of proteins in nuclei appears to require energy (35, 36) and can be inhibited by wheat germ agglutinin (WGA;19). Although RNA export also occurs through the NPC (14, 45), the nature of RNA export signals is not yet known (46). However, tRNA export like protein import is saturable and highly specific; a single base change in human $tRNA_{met}$ reduces export 20-fold (51).

Recently, a family of ~10 immunogenic NPC polypeptides, the nucleoporins, have been identified (5, 6, 26, 27). Tight complexes form between WGA and the nucleoporins because they contain O-linked *N*-acetyl glucosamines (GlcNAcs; see 6, 26, 27). Finlay et al. (19) have demonstrated that the accumulation of nucleoplasmin in WGA-treated rat liver nuclei is inhibited, even after extensive washing, when subsequently assayed in their in vitro assay. Furthermore, both protein import and RNA export are inhibited by a monoclonal antibody which recognizes members of the O-linked GlcNAc family of nucleoporins (17). The O-linked GlcNAc-

Christopher W. Akey's present address is Department of Biophysics, Housman Medical Research Center, Boston University School of Medicine, Boston, MA 02118-2394. David S. Goldfarb's present address is Department of Biology, University of Rochester, Rochester, NY 14627.

1. *Abbreviations used in this paper*: GlcNAc, *N*-acetyl glucosamine; NP, nucleoplasmin; NPC, nuclear pore complex; WGA, wheat germ agglutinin.

containing nucleoporins are likely therefore, to play a critical role in the nuclear transport process.

The mapping of macromolecular binding sites on the nuclear pore was contingent on the application of cryo-electron microscopy of frozen hydrated specimens (12) to the amphibian oocyte system (2). We report herein on the positions within NPCs of the stable binding sites of mAb-414, WGA, and NP conjugated to colloidal gold. The binding sites of these three probes are localized at similar radii, between 100–125 Å and are limited primarily to a central channel-like assembly in the NPC. In addition, the binding sites of WGA and NP may not be mutually exclusive as ascertained from both single and double label experiments, given the physical dimensions of these macromolecules. Furthermore, we have identified at least three distinct types of complex formed between NP-gold and the NPC transporter. We suggest that these complexes represent bound intermediates in a multistep nuclear import pathway. NP-gold may bind initially at multiple, circularly arrayed sites at the periphery of the closed transporter. NP-gold also binds directly over the center of the transporter in a docked configuration. Therefore, peripheral binding to the transporter may represent the staging or holding of excess substrate before docking. Finally, initial experiments suggest that the transporter undergoes a structural rearrangement during the translocation of bound substrate. In support of this hypothesis, we have obtained projection maps of NP-gold docked over the transporter and apparently in transit.

Materials and Methods

Probe Preparation and Microinjection

mAb-414, a mouse monoclonal antibody against a rat liver NPC-lamina fraction (5), was a gift of L. Davis (Whitehead Institute, Cambridge, MA). WGA was obtained from Sigma Chemical Co., St. Louis, MO. NP was prepared from oocytes of *Xenopus laevis* as described (15), using a specific antibody column in the final step. The anti-NP was a gift of C. M. Feldherr (University of Florida, College of Medicine, Gainesville, FL). Colloidal gold sols were prepared using the white phosphorous method for small gold (40–60 Å) and the tannic acid-citric acid method for larger gold sizes (100–150 Å, reference 7). Stabilized colloidal gold probes were prepared from minimal amounts of coating agents and used fresh for all experiments. For the antibody labeling experiments, oocytes from *Necturus* were chosen due to their better overnight storage properties at room temperature. Large oocytes, 2–3 mm in diameter were microinjected with appropriate volumes of mAb-414 to give final intraoocyte concentrations of 10–50 μg/ml. After incubation in situ for 12–16 h, the nuclei were manually extruded into Barths Solution (25), rinsed, labeled with 50 Å protein A-gold (Sigma Chemical Co.), and prepared for cryo-electron microscopy as described below. Freshly stabilized NP-gold probes were microinjected into *Xenopus laevis* oocytes near the midline and nuclei were manually extruded over a period of 15–60 min. The nucleoplasm was clearly red, indicative of transport and this transport could be inhibited by coinjection of excess WGA. Controls to test the specificity of WGA-gold with *Xenopus* nuclei have been reported previously (19). We found that addition of sugar solutions had a deleterious effect on the preparation of frozen hydrated membranes. However, we tested the efficacy of the probe with tissue culture cells exposed to either WGA-gold or WGA-gold and excess GlcNAc. The treated specimens were subsequently embedded, thin sectioned, and checked in the electron microscope. The WGA-gold was found to bind specifically to the plasma membrane and was competed off by excess GlcNAc. Furthermore, Con A-gold showed no binding to regions of *Xenopus* nuclei with intact nuclear membranes.

Specimen Preparation and Cryo-electron Microscopy

Oocytes and nuclei were prepared as described previously (2). Nuclei were subsequently incubated in appropriate solutions: WGA-gold for 3–5 min; NP-gold for 3–10 min; and NP-gold in fresh oocyte extract mixture, 3–10 min. The nuclei were again rinsed by sequential transfer between adjacent drops of low salt buffers (48) and allowed to adhere to suitable electron microscopy support grids which had been previously glow discharged in amyl amine (13). The nuclear envelopes were gently spread over the grid after splitting the nuclei ventrally with a fine, sharp glass needle. The specimens were blotted in a humidity chamber attached to a mechanical guillotine plunger and rapidly frozen in liquid N_2-cooled ethane slush. Specimens were subsequently prepared for cryo-electron microscopy as described (2).

Radial Histogram Distributions and Image Processing

Suitable micrographs as judged by the criteria of ice thickness, specimen preservation, clarity of labeling patterns, proper astigmatism and defocus, and lack of drift were densitometered at an aperture and step size of 25 μm on a Perkin-Elmer Corp. (Norwalk, CT) 1010A densitometer. Histograms of the radial distributions were carried out as follows. Previously selected and windowed NPCs were computationally dusted. This procedure consisted of replacing the gold densities in the images with random density values within the density limits of the particles. The images were then rotationally and translationally aligned for two to three cycles with SPIDER, a modular single particle image processing system (20), with a radial weighting scheme which allowed the rotational alignments to be dominated by the strong features at high radius (i.e., the spokes and membrane border). The alignment parameters were then used to orient the original images with intact gold densities. The radial distances of individual gold probes were measured interactively on a 512 AED graphics screen with programs written for this purpose. The subsequent data were sorted into groups and are presented as histograms in Fig. 4. The NP-gold datasets with centered probes were individually eightfold enforced and displayed on the AED. The entire dataset of 147 particles was further classified into eight classes based on similarity of the transporter-gold probe motifs. Individual classes were averaged and suitable portions were windowed out for figures. In addition, global averages combining comparable classes of staggered and aligned transporters, were calculated after the appropriate angular rotation of ~22.5°, determined by angular correlation for each separate case. The global averages were calculated in the staggered orientation which seems to predominate in this dataset (roughly 2:1). Finally, composite images of NPCs were recreated by adding selected transporter averages with the outer portions of a 450-particle average of NP-gold-labeled NPCs after scaling, thereby maximizing the signal of both the transporter images and the pore complex in one image. All greyscale images were photographed off of a 767 AED using Ilford Ltd. PanF film (Basildon, Essex, England).

Results

Mapping of mAb-414 Epitopes

The suitability of mAb-414 as a probe for members of the O-linked GlcNAc family of nucleoporins was examined by immunofluorescence and Western blotting techniques, using crude NPC–lamina extracts from *Xenopus* A6 tissue culture cells. mAb-414 stained *Xenopus* nuclei in the punctate fashion characteristic of NPC labeling (data not shown) and recognized a prominent 62-kD polypeptide, presumed to be the *Xenopus* counterpart of rat np62, as well as some minor bands on Western blots. However, the number and relative amounts of nucleoporins recognized by mAb-414 may differ in solution due to differences in the presentation of the carbohydrate-containing epitopes (6).

Labeling studies with mAb-414 were performed by microinjecting *Necturus* oocytes with antibody and incubating overnight. The extruded nuclei were subsequently labeled with 50-Å protein A–gold and prepared for cryo-electron microscopy. A typical image is shown in Fig. 1 *a* and a montage of labeled NPCs in Fig. 1 *b*. Because the images are from frozen hydrated specimens, the NPCs have the same contrast as the gold, albeit weaker, and are dark. The observed labeling over the central region of the NPC was consistent and of-

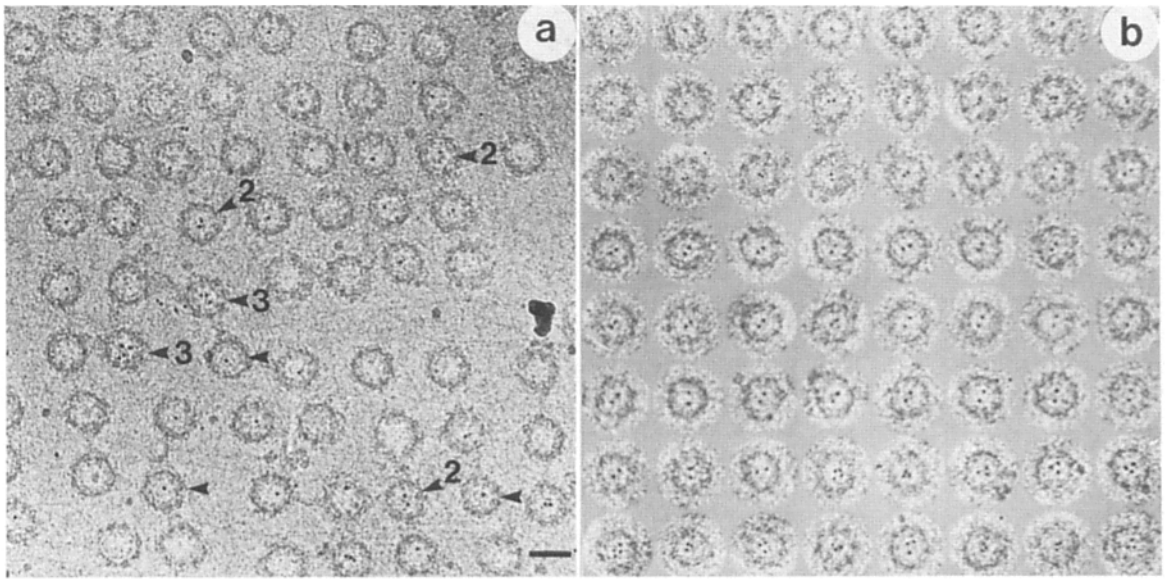

Figure 1. Necturus NPCs labeled with mAb-414 protein A–gold. (*a*) Micrograph of individual NPCs labeled with one, two, or three probes over the central transporter region. The unlabeled arrows indicate NPCs in which the transporter can be observed directly underlying the probes. (*b*) A montage of NPCs labeled with mAb-414 protein A–gold, in which singlet, doublet, triplet, and quadruplet labeling patterns are obvious. Other nonsymmetrical patterns over the transporter were observed but are not included in this analysis. Bars, 1,250 Å.

ten occurred as singlets, doublets, and triplets of gold particles, with a rare quadruplet (see Fig. 1 *b* for a graded series). Nuclei incubated with protein A–gold alone showed no labeling. We believe that this striking pattern arises from bivalent binding of the antibody to flexible epitopes, comprised in part of O-linked GlcNAcs (5, 6), on radially arrayed antigens in the transporter. Calculations suggest that the range of motion of the Fab arms can readily accommodate the circumferential distance between epitopes, located with putative eightfold symmetry in the transporter. A histogram of radial distances from ~100 NPCs labeled with apposed gold particles (see Fig. 4 *a*), demonstrates a major peak at a radius of 100 Å (SD = ±30). The halfwidth of the distribution (~70 Å) is ~50% narrower than that expected for the accepted length of the mAb-414 protein A–gold probe (~150 Å). This may be due to the doubly tethered complex standing up vertically over the transporter, an orientation preserved in amorphous ice. Furthermore, the relative angular position of the doublet golds in the NPCs was investigated after computer-based alignments. However, interpretation of the angular mapping data is complicated by the apparent existence of the transporter in two packing configurations within the pore complex (see section on averages) and the limited specificity of mAb-414 (6). In principle, angular mapping of individual nucleoporins is possible but must await the availability of robust monospecific antibodies and their Fabs.

Mapping the WGA Binding Sites

WGA is a probe specific for the O-linked GlcNAc family of nucleoporins in the NPC–lamina fraction of *Xenopus* (19, 42). Extruded oocyte nuclei were incubated in 60-Å WGA–gold and examples of the resulting labeling patterns are shown in Fig. 2, *a–c*. WGA labeling tends to be circularly symmetric about the center of the transporter (Fig. 2, *a* and *c*, *1*). The micrograph in Fig. 2 *a* is from an atypical area in which a percentage of NPCs showed a circular labeling at higher radii (Fig. 2, *a* and *c*, *2*), as well as the tight labeling pattern (*1*) which was present in >95% of the WGA–gold-labeled specimens. A montage of WGA-labeled NPCs is presented in Fig. 2 *c*. The inset in Fig. 2 *b* shows a single NPC with a circular staining pattern comprised of eight to nine gold particles with a single gold particle over the center of the channel. Specimens incubated in high concentrations of WGA–gold labeled heavily over the entire transporter in a manner similar to high levels of injected NP–gold (18). The radial distributions of both labeling types (Fig. 2, *1* and *2*) were analyzed and a histogram from 340 NPCs is shown in Fig. 4 *b*. Two peaks occur at radii of 125 and 240 Å (SD = ±20) and their positions relative to the components of the NPC are indicated. Only the peak positions are significant, as the distribution is skewed toward the larger radial labeling pattern over what is routinely observed, due to the inclusion of atypical images to obtain accurate statistics for the more rarely observed binding site at higher radius. The in vitro labeling experiment works as the result of a strong affinity of WGA for the O-linked, GlcNAc-containing nucleoporins (the controls are described in Materials and Methods). Some binding of WGA–gold was also observed on NPCs at higher radii over the cytoplasmic ring, between 400 and 600 Å, but was not quantitated.

Mapping NP–Gold Binding Sites

The binding of NP–gold to *Xenopus laevis* nuclear envelopes was investigated following microinjection of NP–gold into living oocytes. Oocyte nuclei were subsequently extruded into buffer over a period of 15–60 min and frozen hydrated specimens prepared. During the course of an experiment, the 60-Å NP–gold accumulated in the nuclei as ascertained by a red staining of the nucleoplasm. Larger NP–gold particles (120–150 Å) showed less nucleoplasmic staining but

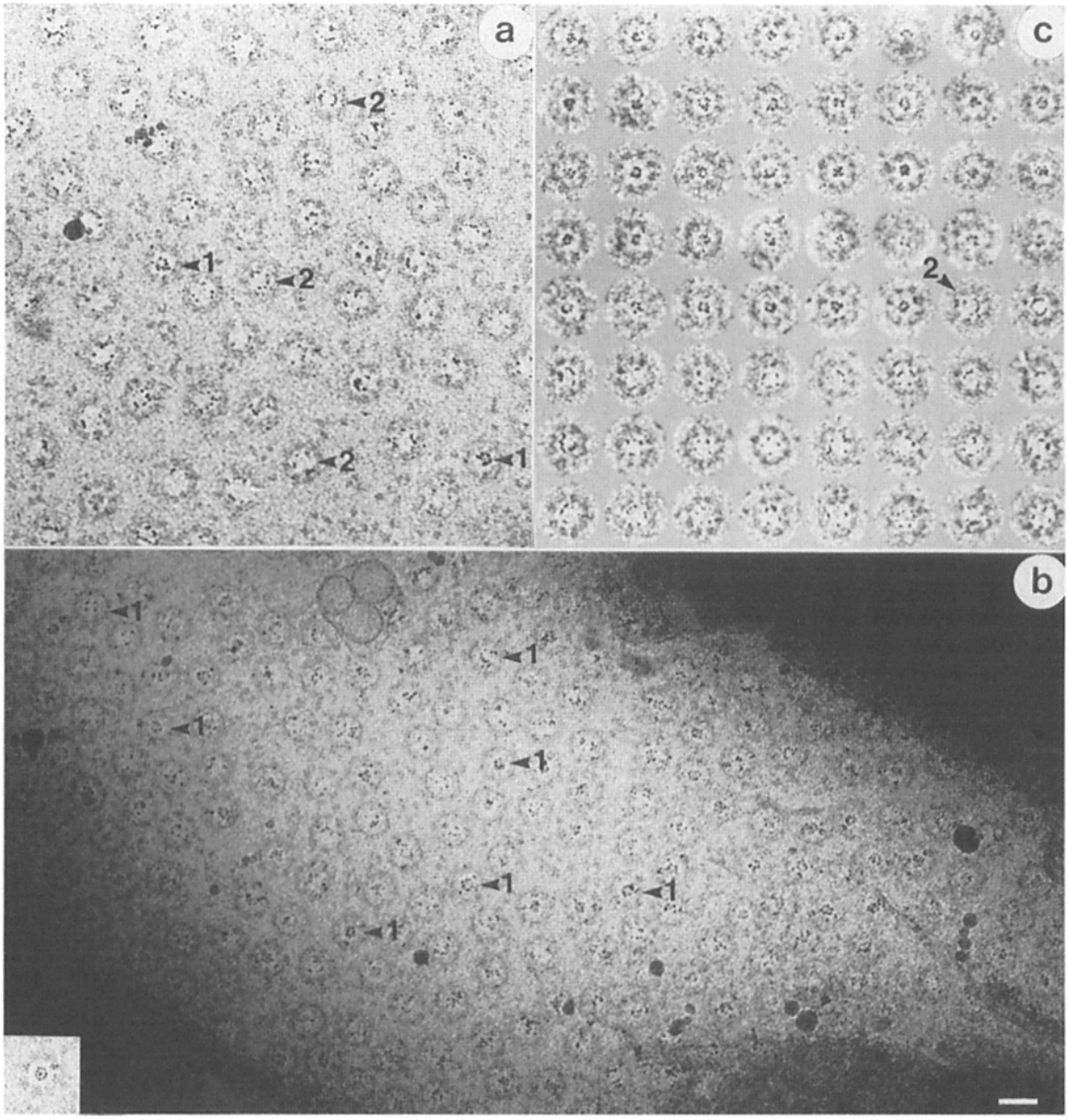

Figure 2. Micrographs and montage of *Xenopus* NPCs labeled with WGA–gold. (*a*) An atypical field of WGA–gold-labeled NPCs in which some labeling at higher radii is observed (*2*), along with the predominant tight labeling pattern (*1*). (*b*) Micrograph of a typical area of WGA-labeled *Xenopus* nuclear envelope in which the type *1* labeling predominates. (*Inset*) A single WGA-labeled NPC which clearly demonstrates that eight or nine very small gold probes can bind circumferentially round the transporter at similar radii, with one or two probes bound centrally. (*c*) Montage of type *1*– and type 2–labeled NPCs. Note that in some cases of type *1* labeling (top four rows), the face of the NPC transporter is saturated. Bars, 1,250 Å.

rather more nuclear envelope staining and a similar NPC localization. Labeling of the nuclear envelopes was heavier nearer the point of microinjection as observed previously in thin sections (18). Images of well preserved, membrane-associated NPCs with subsaturating levels of labeling were selected for analysis in order to facilitate accurate radial measurements of individual gold particles. A field of NP–gold-labeled NPCs is shown in Fig. 3, *a* and *b*. Because the images are from frozen hydrated specimens, the NPCs have the same contrast as the gold, albeit weaker, and are dark. Fig. 3 *a* was recorded at a defocus which optimized the strong scattering from the gold, while Fig. 3 *b* was recorded at a defocus chosen to optimize the contrast of the more weakly scattering NPCs. Various types of labeling patterns were observed indicating the NP–gold binds to the central transporter domain of the NPC. Besides complexes in which the gold resides directly in the center, some transporters are labeled with multiple NP–gold particles, often in a ring pattern but sometimes in dense clusters. The NP–gold labeling pattern is specific for NP, as BSA–gold does not associate similarly (data not shown). After centering alignments, a radial histogram was obtained (Fig. 4 *c*) using a set of interactive programs written to handle the large dataset, ~1,100 measurements from 450 NPCs. The distribution consists of three

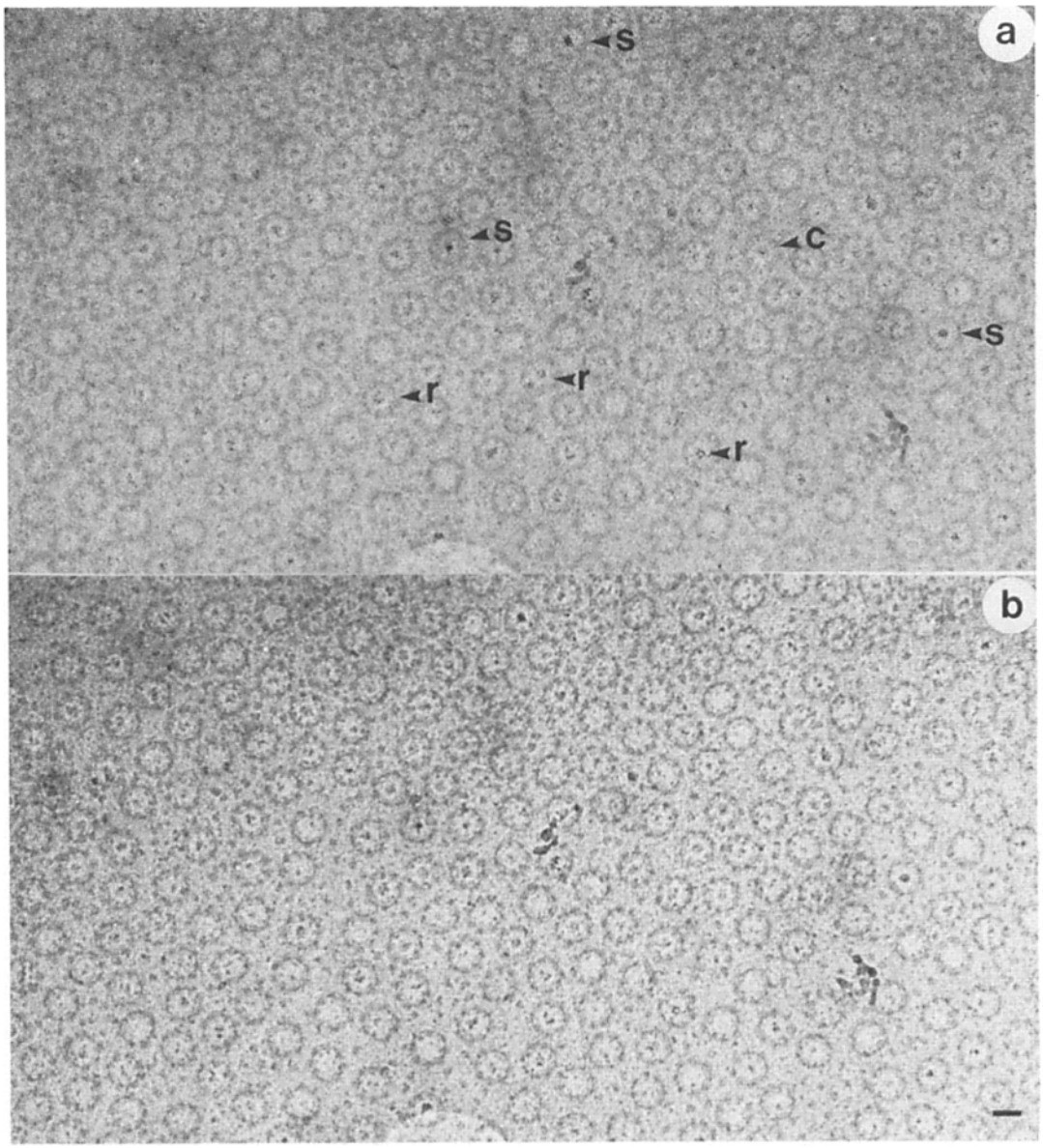

Figure 3. A pair of micrographs of NP-gold-labeled *Xenopus* nuclear envelopes recorded at different values of defocus. (*a*) The gold densities are clearly observed over the central transporter at this defocus. An example of a well-centered gold probe, docked to a visible transporter, is marked *c*. Further examples of ring-like labeling (*r*) and saturated labeling (*s*), similar to that observed with WGA labeling, are indicated. (*b*) Second micrograph recorded at 19.2-μm defocus, to optimize the contrast of the weaker scattering NPCs, relative to the gold probes. Particles presumed to be ribosomes lie scattered in the intervening membrane spaces between NPCs. Bar, 1,000 Å.

peaks at radii of 50, 110, and 400–600 Å (SD = ±30). Significant labeling also occurred directly over the transporter center. The peak at 50 Å radius corresponds to instances where two gold particles were docked side-by-side over the transporter, and to cases where single particles were bound at the edge of the putative central pore. The peak at a radius of 110 Å results mainly from transporters labeled with both single gold particles and particles arrayed in rings or arc sections whose foci are at the transporter center. The prominence of the third peak is misleading due to the bin size. This peak may correspond to weaker labeling over the spokes and cytoplasmic ring of the NPC.

Interestingly, the extensive labeling obtained in vivo by microinjection could not be reproduced by incubating extruded nuclei in buffer containing NP-gold at concentrations effectively 10–20-fold higher than injected. Preliminary reconstitution experiments, in which the NP-gold and nuclei were incubated in a concentrated oocyte extract, did show occasional labeling over the transporter but no labeling at higher radii.

Double Labeling with NP-Gold and WGA-Gold

Because the radial distributions of NP-gold and WGA-gold labeling were similar, we attempted to colocalize these labels within the same NPCs. Newmeyer and Forbes (35) showed that NP-gold retains the ability to bind the cytoplasmic face of NPCs after incubation on the nuclei in WGA. NP-gold

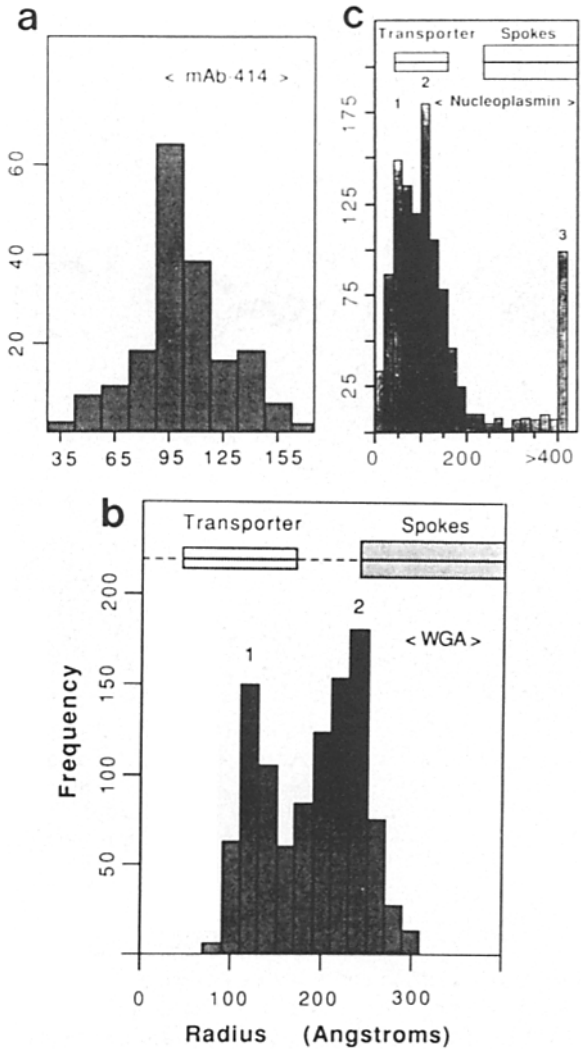

Figure 4. Radial histograms for the three probes used in this study. (*a*) Distribution for NPCs labeled with mAb-414 protein A–gold in centro-symmetric doublet patterns. The peak occurs at 95–105 Å. The halfwidth of the peak is ~50 Å. (*b*) Distribution of NPCs labeled with WGA–gold. Two peaks are observed: type *1* centered at 125 Å and type *2* at 240 Å. The type *2* labeling is rarely observed in well-preserved specimens. (*c*) Distribution of NP-gold on NPCs. The three peaks are described in the text.

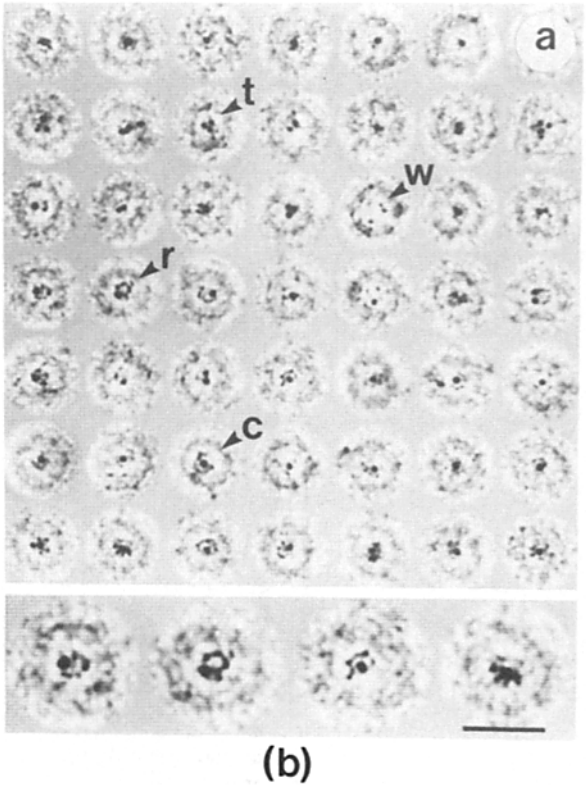

Figure 5. (*a*) Montage of *Xenopus* NPCs double labeled with large NP–gold in vivo, followed by small WGA–gold in vitro. First three rows show NPCs labeled with one, two, and three large NP–golds. An NPC with three WGA–gold labels is marked *t*. The NPC labeled *w* is labeled with small WGA–gold (from the same original micrograph). The next 12 particles show coradial labeling of the two probes over the transporter (marked *r*). The bottom two rows, labeled *c*, demonstrate a centrally docked NP–gold bounded circumferentially by small WGA–golds at a radius of ~120–140 Å. (*b*) Enlarged images of select double-labeled NPCs. The apparent diameter of the NPCs corresponds to 1,200 Å. Bar, 1,200 Å.

(100–150 Å) was microinjected into oocytes and within 60 min the nuclei were extruded into buffer containing WGA–gold (50–60 Å). A montage of double-labeled NPCs is shown in Fig. 5 *a* and a few enlarged fields in Fig. 5 *b*. In the montage the top three rows contain examples of single, double, and triple labeling with the large NP–gold. The panel labeled *w* shows a circular labeling by the smaller WGA–gold. The row of particles labeled *r* shows NPCs in which the NP–gold and WGA–gold labels are coradially aligned over the transporter. The next three rows show examples in which the NP–gold is located over the center of the transporter, while the WGA–gold is bound circumferentially. Thus, NP and WGA can bind simultaneously at similar radial binding sites, within the resolution of this study. Therefore, NP may bind directly to certain GlcNAc-containing nucleoporins; however, the experiment does not eliminate the possibility that nucleoplasmin binds to receptors localized adjacent to the GlcNAc-containing nucleoporins in the transporter assembly. An interpretation of the labeling studies is given in the Discussion. However, observation of the second class of double labeling seems to indicate that the association of NP with the transporter is stable over the 5–10 min required to prepare the specimens in the absence of cross-linking.

Averages of NPCs Labeled with NP–Gold

Selected images of NP–gold-labeled NPCs were densitometered, aligned, and averaged using SPIDER, a single particle image processing program (20). The structure of membrane-associated NPCs preserved in amorphous ice is described in the accompanying paper (2). However, the major features of the pore complex including the membrane border and the octagonally symmetric spokes are well preserved in the NP–gold-labeled images. In these images (see Fig. 6, *a* and *b*), regions of high density (protein and gold) are white. A 200-particle data set was selected from ~20 micrographs in which single NP–gold particles were bound within ~50 Å

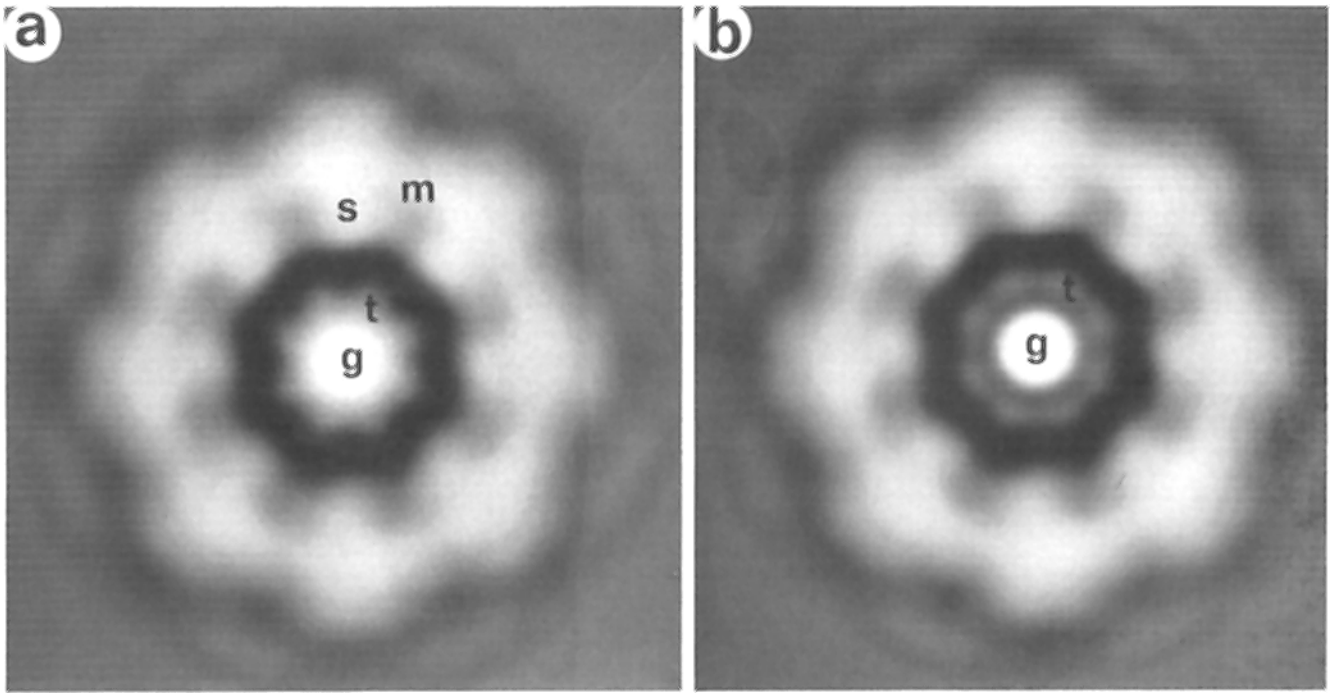

Figure 6. Averages from 450 NPCs in frozen buffers, originally labeled with NP–gold over their transporters before computer-based averaging. The quality of the outer portion of the maps indicates that labeling and subsequent specimen preparation has not significantly altered the structure of the NPC over what is normally observed (see reference 2). The spokes and membrane border are labeled (*s* and *m*). (*a*) A composite image showing the staggered packing relationship between the outer portion of the pore complex and the transporter. The transporter has NP–gold docked over it. (*b*) Similar image to that in *a* showing the transporter with NP–gold apparently caught in transit.

of the center of the transporter. After a cycle of computer alignment, some NPCs were discarded due to the presence of previously undetected double labeling or as the result of unacceptably large radial misalignments. A final dataset of 147 eightfold-averaged NPCs was then subjected to three cycles of manual classification into eight classes with similar structural motifs in the central assembly. Features of the pore complex in the various class averages were very similar (data not shown).

Two composite images are shown in Fig. 6, *a* and *b*. The projection maps exhibit a significant difference in the distribution of protein density (Fig. 6, *white areas*) about the central transporter assembly. The image in Fig. 6 *a* shows centrally located NP–gold docked over a transporter whose structure is otherwise indistinguishable from that of unlabeled and presumably closed transporters. (C. W. Akey, unpublished data). The transporter in Fig. 6 *b* appears to have opened forming a region of negative (Fig. 6 *b*, *black center ring*) density around the NP–gold. The NP–gold particles associated with the transporter have apparently been caught in the act of translocation. A montage of projection maps of the eight classes is shown in Fig. 7. Note that in Fig. 7 only the transporter is presented, not the entire NPC. The 12 averages in Fig. 7 are presented in columns of staggered (*S*), aligned (*A*), and global averages (*G*) ($G = S + A$, after a 22.5° rotation of *A*), with alternate rows showing docked and possible "in transit" forms. A third level of classification has also been introduced with the first two rows corresponding to maps of smaller NP–gold particles over the transporter while the last two rows correspond to maps with larger NP–gold particles or unresolved aggregates. There is good agreement between transporter features of the various averages in similar configurations, as well as among the global averages. Interestingly, the radius of the apparent channel is variable and correlated to the radius of the NP–gold particle complexed with it.

Overall, the analysis revealed two structural motifs relevant to the function of the transporter assembly. First, the closed transporter with NP–gold docked at the center displays a star-like shape while the transporter with NP–gold apparently in transit displays a characteristic annulus of densities, a structure which is qualitatively different from the docked form. Second, the packing of the transporter within the pore complex appears to be polymorphic, occurring in two configurations which differ by 22.5°. Relative to the octagonally symmetric spokes of the pore complex, the arrangement of the morphological subunits of the transporter can be described as being either aligned (Fig. 7, *A*) or staggered (Fig. 7, *S*). The 22.5° angular difference in packing may reflect both possible configurations of the transporter with respect to the two unique twofold axes which exist in the pore complex which has 822 symmetry (2, 32).

Evidence of a phase-contrast ring, an imaging artifact associated with the diminution of low frequency components in the specimen during imaging, was not observed around the strongly scattered gold particles in the averaged maps. This may have resulted from an inherent variability in radial positioning of the gold probes over the transporter, due to the geometry of binding sites on the gold particles. Small positional errors of the gold probes with respect to the particle

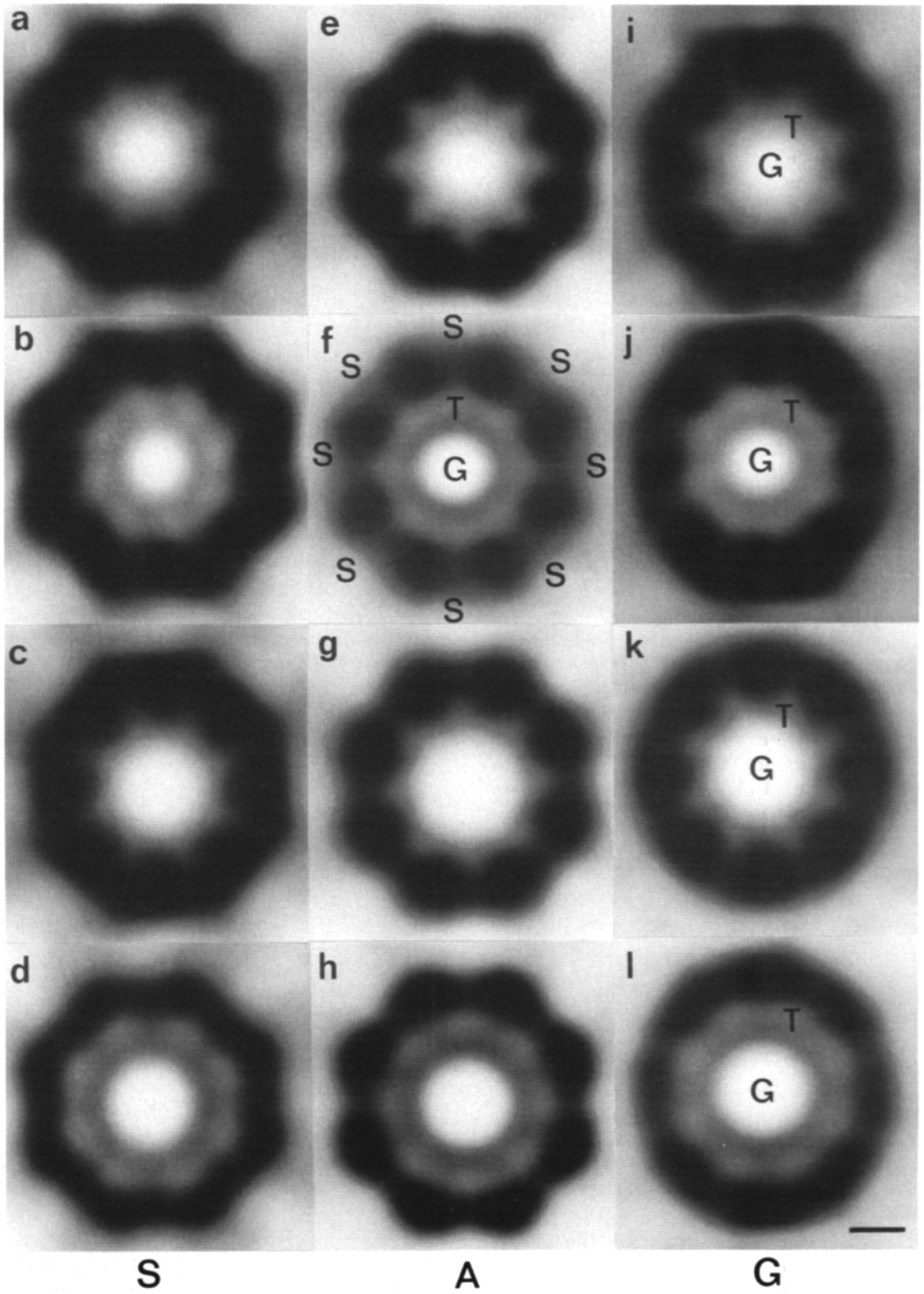

Figure 7. Montage of projection maps of NP-gold-labeled NPC transporters from the eight classes described in the text. Global averages are also shown. The columns correspond respectively to staggered (*S*), aligned (*A*), and global averages (*G*). The rows are grouped into small gold (first two) and larger gold (last two). Each of these is further subdivided into a docked and in transit row. For example, *d* corresponds to an average of transporters with larger NP-gold apparently caught in transit which are packed in the pore complex in a staggered orientation (see text). The number of particles in each class (*a–l*) is respectively: 44, 12, 20, 18, 14, 8, 15, 16, 58, 20, 35, and 34. Bar, 100 Å.

centers would tend to average the gold particle phase ring with the much stronger edge density from the slightly misaligned gold particles, as the centering alignments were based on the strong eightfold features of the pore complex. In addition, the observation of the weak protein density of the transporter in similar docked and in transit configurations for different sized populations of bound gold probes, when combined with the dissimilarity of the two structures, serves as an internal control and suggests that the observed changes in the transporter may be associated with transport. Calculations indicate that the angular orientation of features at the particle centers will be correct providing that a suitable defocus is used in recording the micrographs, as was done in this study (see reference 2). Finally, the selection criteria used in these experiments, the presence of a central gold probe, insured that the transporters in the chosen NPCs were well ordered. This data therefore provides initial structural evidence on the mechanism of transport through the nuclear pore. However, further structural data in two and three dimensions are needed to corroborate these observations.

Discussion

In this study, we have combined colloidal gold labeling, cryo-electron microscopy, and image analysis to map the radial positions of sites which are potentially relevant to nuclear import. The three probes used in this work have enabled us to map the positions of the following: epitopes recognized by mAb-414, which include the O-linked GlcNAc-containing nucleoporins np62 and np175; a high affinity WGA binding site and possible site of transport inhibition; and the binding sites of NP, a transport substrate. The major binding sites of these probes occur at similar radii, between 100 and 125 Å on the NPC transporter and are circularly arrayed. As shown herein and by others (15, 18, 21, 45), NPC-mediated transport appears to occur through a constriction at the level of the central spokes. Furthermore, the central transport assembly is ~390 Å in diameter while WGA and NP have maximal dimensions of ~70 and 80 Å, respectively (8, 49). Therefore, the sizes of the gold-labeled probes, including protein coats (total diameter, ~80 Å), are similar to the largest dimensions of the biologically active forms of the probe macromolecules; hence, the accuracy of labeling achieved in this study should give results relevant to nuclear transport in the cell.

Peripheral Binding to the NPC Transporter

The simultaneous association of karyophilic protein–colloidal gold probes with multiple sites on the cytoplasmic face of the NPC is well established (18, 35, 40). However, in these studies the observed multiple binding sites of the gold probes could not be accurately mapped on the NPC due in part to the preparative methods used. In the present study, it is apparent that NP can bind to multiple sites on the central transporter. Furthermore, the structure of the pore complexes has been minimally perturbed as reflected by the accuracy of determination of the gold probe positions and the preservation of structural features of the NPC (2). Binding of karyophilic gold over the outermost portions of the NPC between radii of ~400–600 Å has been previously shown to be signal sequence dependent and independent of ATP (35). The apparent discrepancy in location of transportable substrate–gold complexes may be due to differences in specimen preparation or alternatively, may reflect kinetic differences in the trapping of labeled substrate. We point out that our results with WGA and mAb-414 are internally consistent and that the rapidity of specimen preparation combined with the ability to monitor the preservation of the NPCs strongly suggests that our localization methods are reliable. However, the method is clearly dependent on the stability of the NPC–probe complexes and less stable interactions may not be fully represented in our data. This does not pose a problem in the current study as we have chosen to focus on strong binding events at the center of the NPC. Moreover, our results are in agreement with the previously observed transport of NP–gold through the center of the NPC (18). As shown previously (2, 48), the cytoplasmic rings have inner radial boundaries of 400–450 Å. Therefore, the specific labeling observed herein at a radius of ~100–125 Å is likely to occur at the level of the central waist of the spoke assembly.

The nature of the peripheral binding sites on the transporter was further investigated using WGA and mAb-414 as probes for the GlcNAc-containing nucleoporins. Both of these probes indicate that there are GlcNAc-containing nucleoporins localized to the transporter; however, this does not rule out the possibility that some members of this family may have dynamic associations with the NPC. In addition, Scheer et al. (42) have shown by thin section electron microscopy that 100-Å WGA–gold binds to the central regions of *Xenopus* NPCs, as viewed in cross sections. Furthermore, double labeling of NPCs with NP–gold and WGA–gold and quantitative mapping indicate that both probes form complexes with the transporter at similar radii. These results are consistent with the hypothesis that the nucleoporins may ". . . constitute or are part of receptors for transporting different classes of macromolecules between the nucleus and cytoplasm" (Snow et al.; reference 44). Alternatively, the peripheral transporter binding sites may be unidentified proteins which reside adjacent to the nucleoporins in the transporter. No matter how closely NP–gold peripheral binding sites and the GlcNAc-containing nucleoporins can be colocalized within the transporter, a functional role for these nucleoporins in signal recognition must await biochemical and genetic tests.

Taken together, the data suggest that peripheral binding to the transport assembly is an early step along the nuclear transport pathway which may be preceded by cytoplasmic transport (40) and possible substrate binding to the cytoplasmic rings (35). Multimeric proteins such as NP and SV-40 large T antigen may increase their ability to compete for NPC binding sites by virtue of their multiple signal sequences. Tighter binding (lower K_d) of transport substrates would be expected if multiple signal sequences could be bound simultaneously by multiple receptors. Both the association of karyophilic substrates with the nuclear envelope and their rate of accumulation in nuclei are influenced by the multiplicity of signal sequences displayed by individual substrate molecules (11, 15, 31). We have observed both specific radial binding to the NPC transporter and nuclear import of 60-Å gold particles stabilized with BSA coupled to high numbers of mutant peptides, which contain a threonine as replacement for lysine-128 in the SV-40 large T antigen signal sequence; a low multiplicity of peptides resulted in poor

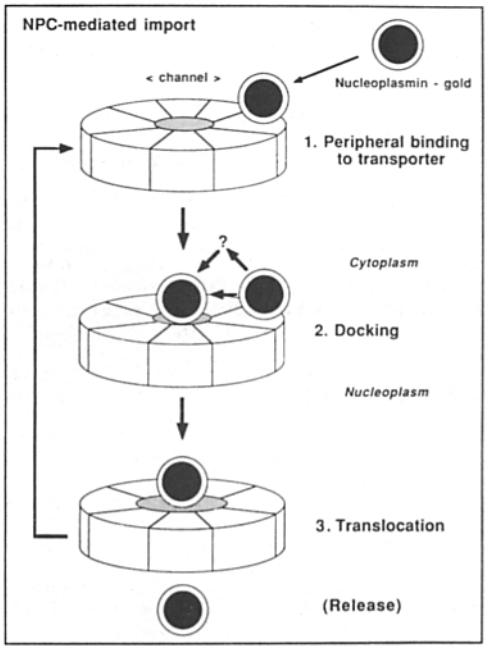

Figure 8. A possible three-step mechanism of nuclear import at the level of the NPC transporter is presented. The data shown in Figs. 6 and 7 when combined with the labeling results leads to a simple model of nuclear import involving: (*1*) specific binding of transport substrates at the perimeter of the transporter (radius, 100–125 Å), possibly involving O-linked GlcNAc-containing nucleoporins; (*2*) docking of substrate over the center of the closed transporter; and (*3*) opening of the transporter resulting in translocation, possibly followed by a release step. The translocation step is shown schematically as a dilation of the transporter; however, the actual mechanism is not known.

transport (15, 23). Therefore, multivalent effects may play a role in the binding and translocation phases of nuclear import.

Docking

In addition to peripheral binding, NP–gold is observed to bind directly over the center of the transporter. Although not in itself surprising, as protein import through the center of the NPC was first shown by Feldherr et al. (18), the observation of both docked complexes and probes apparently in transit (21, 45), suggests the formation of a minimum of three distinct, centrally localized substrate–NPC complexes during transport. These include (*a*) substrate docking at the center of the pore complex which may be preceded by peripheral binding, (*b*) gating of the central assembly to accommodate substrate by an as yet undetermined mechanism, and (*c*) translocation of substrate through the nuclear pore coupled with release of the substrate (see Fig. 8). Similar pathways have been proposed (35); however, we provide evidence in support of distinct binding, docking, and translocation complexes at the level of the central NPC transporter. What is the relationship between binding and docking on the transporter? Peripheral binding sites may be staging or holding complexes which precede the concerted transfer of substrates across the surface of the transporter to the docking site(s). Alternatively, peripheral binding sites could represent unproductive complexes which must dissociate before docking. We were unable to obtain either peripheral binding or docking by incubating extruded nuclei in buffer laced with NP–gold. This result indicates that some necessary component, either a soluble factor or an integral component of the NPC, was lost during extrusion of nuclei. However, labeling was observed occasionally when nuclei were extruded into NP–gold suspended in concentrated oocyte extracts. Recently, Adams et al (1) have identified two putative signal sequence–binding proteins which may potentially participate in the docking and translocation reactions.

Translocation

The maps presented in Figs. 6 and 7 suggest that the fundamental mechanism of NPC-mediated transport may involve the opening of a central assembly within the NPC to facilitate translocation. More than a decade ago, Bonner (4) hypothesized that large proteins might enter the nucleus by increasing the nuclear pore radius through specific interactions or alternatively, by becoming asymmetric to allow passage through a fixed pore. More recently, studies with karyophilic gold argue against the deformation hypothesis for proteins (18). A salient feature of the triple ring model of NPC architecture proposed by Unwin and Milligan (48) is a central granule or plug whose function is unknown (21). However, it has been postulated that the central granule may represent endogenous substrates caught in transit during specimen preparation. Centrally located channel-like features have been observed in individual NPCs and in averages of detergent-extracted NPCs (2). In the present model, a centrally located transport assembly opens to accommodate substrates. It is not known if the putative channel is a variably gated pore through which substrates diffuse or, alternatively, a receptor-lined cylinder involved in active translocation. Hence, the translocation step depicted in Fig. 8 is meant to be schematic and does not imply a specific mechanism. We propose that the term NPC transporter be applied to this unique and dynamic assembly.

These experiments revealed two other aspects of transporter structure and function. First, the radial labeling patterns of WGA and mAb-414 suggest that accessible GlcNAc-containing nucleoporins are localized to the central assembly at some point in the transport cycle. Indeed, the nucleoporins recognized by mAb-414 may have become trapped at the transporter during the overnight incubation in vivo; however, short incubations in vitro with WGA–gold gave similar labeling patterns over all the NPCs in an image field, indicating that the GlcNAc-containing nucleoporins may be preferentially bound to the transporter. Second, labeling with mAb-414 and protein A–gold displayed unusual features consistent with the hypothesis that some members of the nucleoporin family are distributed around the transporter with eightfold symmetry. In addition, WGA labeling with either 60-Å gold (this work) or 100-Å gold (42) suggests that there are four to eight binding sites on the transporter located at similar radii. This data indicates that the accessible half of the transporter may be comprised of at least eight subunits which act in concert during translocation.

The antinucleoporin antibody RL1 has been shown to inhibit NP import after microinjection into oocytes, without impeding the transit of small molecules through the pore complex (17). One possible mechanism of inhibition may in-

volve cross-linking of adjacent nucleoporins, thereby disrupting the transport sequence. Indeed, WGA may inhibit transport by this mechanism as the passive diffusion of small dextrans and nonkaryophilic proteins into the nucleus was not blocked by microinjected WGA (50). WGA is known to bind efficiently as a bivalent ligand and given its size (40 × 40 × 70 Å) and the positions of sugar binding sites in WGA (47), coupled with the radial location of the WGA binding sites on the transporter, it seems plausible that WGA could physically cross-link adjacent subunits on the cytoplasmic face of the transporter. The major focus of this interaction may be with np62 and np175, although interactions with other O-linked GlcNAc-containing nucleoporins cannot be ruled out. A second potential mechanism of transport inhibition might involve competitive binding of WGA with transport substrates on the transporter (34). However, if the subunit cross-linking mechanism is correct, roughly one bound WGA per transporter would be sufficient to shut down transport, thereby leaving a large number of unoccupied substrate binding sites. A third potential mechanism of transport inhibition may involve specific inactivation of a transport-dependent NTPase (3).

Conclusions

We have presented data which supports a sequential model of nuclear import involving peripheral binding to the NPC transporter, substrate docking, translocation, and subsequent release. The observed coradial binding of NP, WGA, and mAb-414 suggests that the GlcNAc-containing nucleoporins may indeed play a role in the nuclear transport process. Furthermore, the sequential model of transport presented herein is likely to be part of a nuclear import pathway which uses specific macromolecules to regulate transport (8, 22, 24, 37), as demonstrated recently by the identification of two soluble, nuclear localization sequence-binding proteins by Adams et al. (1). Our inability to reconstitute NP-gold binding to extruded nuclei under conditions where WGA binding was competent, coupled with observations from the mapping and double-labeling experiments that their binding sites may overlap radially, would seem to support this concept.

We wish to thank Drs. P. N. T. Unwin and R. Kornberg for their support, Dr. C. Feldherr for materials and advice, Dr. L. Davis for mAb-414, and Lynne Mercer for thin section work.

This work was supported by grants and fellowships from the National Institutes of Health (to C. W. Akey, D. S. Goldfarb, R. Kornberg, and P. N. T. Unwin) and the California Division of the American Cancer Society (to D. S. Goldfarb).

Received for publication 26 January 1989 and in revised form 1 June 1989.

References

1. Adams, S. A., T. J. Lobl, M. A. Mitchell, and L. Gerace. 1989. Identification of specific binding proteins for a nuclear localization sequence. *Nature (Lond.).* 337:276–279.
2. Akey, C. W. 1989. Interactions and structure of the nuclear pore complex revealed by cryo-electron microscopy. *J. Cell Biol.* 109:955–970.
3. Baglia, F. A., and G. G. Maul. 1983. Nuclear RNP release and nucleoside triphosphatase activity are inhibited by antibodies to a nuclear matrix glycoprotein. *Proc. Natl. Acad. Sci. USA.* 80:2285–2289.
4. Bonner, W. M. 1978. Protein migration and accumulation in nuclei. *In* The Cell Nucleus. H. Busch, editor. Vol. 6, Part C. Academic Press, New York. 97–148.
5. Davis, L. I., and G. Blobel. 1986. Identification and characterization of a nuclear pore complex protein. *Cell.* 45:699–709.
6. Davis, L. I., and G. Blobel. 1987. Nuclear pore complex contains a family of glycoproteins that includes p62: glycosylation through a previously unidentified cellular pathway. *Proc. Natl. Acad. Sci. USA.* 84:7552–7556.
7. De Mey, J., and M. Moeremans. 1986. The preparation of colloidal gold probes and their use as marker in electron microscopy. *Adv. Tech. Biol. Electron Microsc.* 3:229–266.
8. Dingwall, C., and R. A. Laskey. 1986. Protein import into the cell nucleus. *Annu. Rev. Cell Biol.* 2:367–390.
9. Dingwall, C., S. M. Dilworth, S. J. Black, S. E. Kearsey, L. S. Cox, and R. A. Laskey. 1987. Nucleoplasmin cDNA sequence reveals polyglutamic acid tracts and a cluster of sequences homologous to putative nuclear localization signals. *EMBO (Eur. Mol. Biol. Organ.) J.* 6:69–74.
10. Dingwall, C., J. Robbins, S. M. Dilworth, B. Roberts, and W. C. Richardson. 1988. The nucleoplasmin nuclear localization sequence is larger and more complex than that of SV-40 large T antigen. *J. Cell Biol.* 107: 841–849.
11. Dingwall, C., S. V. Sharnick, and R. A. Laskey. 1982. A polypeptide domain that specifies migration of nucleoplasmin into the nucleus. *Cell.* 30:449–458.
12. Dubochet, J., M. Adrian, J. Chang, J. C. Homo, J. Lepault, A. W. McDowall, and P. Schultz. 1988. Cryo-electron microscopy of vitrified specimens. *Quatr. Rev. Biophys.* 21:129–228.
13. Dubochet, J., M. Groom, and S. Mueller-Neuteboom. 1982. Mounting macromolecules for electron microscopy with particular reference to surface phenomena and the treatment of support films by glow discharge. *Adv. Opt. Electron Microsc.* 8:107–135.
14. Dworetzky, S. I., and C. M. Feldherr. 1988. Translocation of RNA-coated gold particles through the nuclear pores of oocytes. *J. Cell Biol.* 106:575–584.
15. Dworetzky, S. I., R. E. Lanford, and C. M. Feldherr. 1988. The effect of variations in the number and sequence of targeting signals on nuclear uptake. *J. Cell Biol.* 107:1279–1288.
16. Deleted in proof.
17. Featherstone, C., M. Darby, and L. Gerace. 1988. A monoclonal antibody against the nuclear pore complex inhibits nucleocytoplasmic transport of protein and RNA in vivo. *J. Cell Biol.* 107:1289–1297.
18. Feldherr, C. M., E. Kallenbach, and N. Schultz. 1984. Movement of a karyophilic protein through the nuclear pores of oocytes. *J. Cell Biol.* 99:2216–2222.
19. Finlay, D. R., D. D. Newmeyer, T. M. Price, and D. J. Forbes. 1987. Inhibition of in vitro nuclear transport by a lectin that binds to nuclear pores. *J. Cell Biol.* 104:189–200.
20. Frank, J., B. Shimkin, and H. Dowse. 1981. SPIDER a modular software system for electron image processing. *Ultramicroscopy.* 6:343–358.
21. Franke, W. W. 1974. Structure, biochemistry and functions of the nuclear envelope. *Int. Rev. Cytol.* 4(Suppl.):71–236.
22. Gerace, L., and B. Burke. 1988. Functional organization of the nuclear envelope. *Annu. Rev. Cell Biol.* 4:335–374.
23. Goldfarb, D. S. 1988. Karyophilic peptides: applications to the study of nuclear transport. *In* Nucleocytoplasmic Transport. R. Peters, editor. Academic Press, Ltd., London. 145–168.
24. Goldfarb, D. S., J. Gariepy, G. Schoolnik, and R. D. Kornberg. 1986. Synthetic peptides as nuclear localization signals. *Nature (Lond.).* 322: 641–644.
25. Gurdon, J. B. 1976. Injected nuclei in oocytes: fate, enlargement and chromatin dispersal. *J. Embryol. Exp. Morphol.* 36:523–540.
26. Hanover, J. A., C. K. Cohen, M. C. Willingham, and M. K. Park. 1987. O-linked *N*-acetyl glucosamine is attached to proteins of the nuclear pore: evidence for cytoplasmic glycosylation. *J. Biol. Chem.* 262:9887–9894.
27. Holt, G. D., C. M. Snow, A. Senior, R. S. Haltiwanger, L. Gerace, and G. W. Hart. 1987. Nuclear pore complex glycoproteins contain cytoplasmically disposed O-linked *N*-acetyl glucosamine. *J. Cell Biol.* 104: 1143–1156.
28. Deleted in proof.
29. Kalderon, D., W. S. Richardson, A. F. Markham, and A. E. Smith. 1984. Sequence requirements for nuclear location of simian virus 40 large T-antigen. *Nature (Lond.).* 311:33–38.
30. Kalderon, D., B. L. Roberts, W. D. Richardson, and A. E. Smith. 1984. A short amino acid sequence able to specify nuclear location. *Cell.* 39:499–509.
31. Lanford, R. E., R. G. White, R. D. Dunham, and P. Kanda. 1988. The effect of basic and nonbasic amino acid substitutions on transport induced by SV40 T-antigen synthetic peptide nuclear transport signals. *Mol. Gen. Genet.* 8:2722–2729.
32. Milligan, R. A. 1986. A structural model for the nuclear pore complex. *In* Nucleocytoplasmic Transport. R. Peters and M. Trendelenburg, editors. Springer-Verlag, New York. 113–122.
33. Milligan, R. A., A. Brisson, and P. N. T. Unwin. 1984. Molecular structure determination of crystalline specimens in frozen aqueous solutions. *Ultramicroscopy.* 13:1–10.
34. Moreland, R. B., G. L. Langevin, R. H. Singer, R. L. Gerace, and L. M. Hereford. 1987. Amino acid sequences that determine the nuclear localization of yeast histone 2B. *Mol. Cell. Biol.* 7:4048–4057.
35. Newmeyer, D. D., and D. J. Forbes. 1988. Nuclear import can be sepa-

rated into distinct steps in vitro: nuclear pore binding and translocation. *Cell.* 52:641–653.
36. Newmeyer, D. D., J. M. Lucocq, T. R. Burglin, and E. M. De Robertis. 1986. Assembly in vitro of nuclei active in nuclear protein transport: ATP is required for nucleoplasmin accumulation. *EMBO (Eur. Mol. Biol. Organ.) J.* 5:501–510.
37. Newport, J. W., and D. J. Forbes. 1987. The nucleus: structure, function and dynamics. *Annu. Rev. Biochem.* 56:535–565.
38. Paine, P. L., L. C. Moore, and S. B. Horowitz. 1975. Nuclear envelope permeability. *Nature (Lond.).* 254:109–114.
39. Peters, R. 1986. Fluorescence microphotolysis to measure nucleocytoplasmic transport and intracellular mobility. *Biochim. Biophys. Acta.* 864: 305–359.
40. Richardson, W. D., A. D. Mills, S. M. Dilworth, R. A. Laskey, and C. Dingwall. 1988. Nuclear protein migration involves two steps: rapid binding at the nuclear envelope, followed by slower translocation through nuclear pores. *Cell.* 52:655–664.
41. Rihs, H.-P., and R. Peters. 1989. Nuclear transport kinetics depend on a phosphorylation site containing sequences flanking the karyophilic signal of the Simian virus 40 T-antigen. *EMBO (Eur. Mol. Biol. Organ.) J.* 8:1479–1484.
42. Scheer, U., M.-C. Dabauvalle, H. Merkert, and R. Benevente. 1988. The nuclear envelope and the organization of the pore complexes. *In* Nucleocytoplasmic Transport. R. Peters, editor. Academic Press, Ltd., London. 5–25.
43. Smith, A. E., D. Kalderon, B. L. Roberts, W. H. Colledge, M. Edge, P. Gillett, A. Markham, E. Paucha, and W. D. Richardson. 1985. The nuclear location signal. *Proc. R. Soc. Lond. B. Biol. Sci.* 226:43–58.
44. Snow, C. M., A. Senior, and L. Gerace. 1987. Monoclonal antibodies identify a group of nuclear pore complex glycoproteins. *J. Cell Biol.* 104:1143–1156.
45. Stevens, B. J., and H. Swift. 1966. RNA transport from nucleus to cytoplasm in Chironomus salivary glands. *J. Cell Biol.* 31:55–77.
46. Tobian, J. A., L. Drinkard, and M. Zasloff. 1985. tRNA nuclear transport: defining the critical regions of human tRNAmet by point mutagenesis. *Cell.* 43:415–422.
47. Unwin, P. N. T., and R. Henderson. 1975. Molecular structure determination by electron microscopy of unstained crystalline specimens. *J. Mol. Biol.* 94:425–440.
48. Unwin, P. N. T., and R. A. Milligan. 1982. A large particle associated with the perimeter of the nuclear pore complex. *J. Cell Biol.* 93:63–75.
49. Wright, C. S. 1977. The crystal structure of wheat germ agglutinin at 2.2 angstroms resolution. *J. Mol. Biol.* 111:439–457.
50. Yoneda, Y., N. Imamoto-Sonobe, M. Yamaizumi, and T. Uchida. 1987. Reversible inhibition of protein import into the nucleus by wheat germ agglutinin injected into cultured cells. *Exp. Cell Res.* 173:586–595.
51. Zasloff, M. 1983. tRNA transport from the nucleus in a eukaryotic cell: carrier-mediated translocation process. *Proc. Natl. Acad. Sci. USA.* 80:6436–6440.